

Neutrino-Nucleus Reactions and Muon Capture in ^{12}C

F. Krmpotić^{1,2,3}, A. Samana¹ and A. Mariano^{2,4}

¹*Instituto de Física, Universidade de São Paulo, 05315-970 São Paulo-SP, Brazil*

²*Instituto de Física La Plata, CONICET, 1900 La Plata, Argentina*

³*Facultad de Ciencias Astronómicas y Geofísicas,
Universidad Nacional de La Plata, 1900 La Plata, Argentina, and*

⁴*Departamento de Física, Universidad Nacional de La Plata,
C. C. 67, 1900 La Plata, Argentina*

Abstract

The neutrino-nucleus cross section and the muon capture rate are discussed within a simple formalism which facilitates the nuclear structure calculations. The corresponding formulae only depend on four types of nuclear matrix elements, which are currently used in the nuclear beta decay. We have also considered the non-locality effects arising from the velocity-dependent terms in the hadronic current. We show that for both observables in ^{12}C the higher order relativistic corrections are of the order of $\sim 5\%$ only, and therefore do not play a significant role. As nuclear model framework we use the projected QRPA (PQRPA) and show that the number projection plays a crucial role in removing the degeneracy between the proton-neutron two quasiparticle states at the level of the mean field. Comparison is done with both the experimental data and the previous shell model calculations. Possible consequences of the present study on the determination of the $\nu_\mu \rightarrow \nu_e$ neutrino oscillation probability are briefly addressed.

PACS number: 13.75.Gx, 14.20.Gk, 13.40.Em

Keywords: neutrino-nucleus cross section, muon capture, projected QRPA

I. INTRODUCTION

The semileptonic weak interactions with nuclei include a rich variety of processes, such as the neutrino (antineutrino) scattering, charged lepton capture, e^\pm decays, etc, and we have at our disposal the results of more than a half-century of beautiful experimental and theoretical work. At the time being their study is mainly aimed to inquire on possible exotic properties of the neutrino associated with its oscillations and massiveness by means of exclusive and inclusive scattering processes on nuclei, which are often used as neutrino detectors. An example is given by the recent experiments performed by both the LSND [1, 2] and the KARMEN [3] Collaborations, looking for $\nu_\mu \rightarrow \nu_e$ and $\tilde{\nu}_\mu \rightarrow \tilde{\nu}_e$ oscillations with neutrinos produced by accelerators. When the ν_e come from decay-at-rest (DAR) of μ^+ the flux contains neutrinos with a maximum energy of 50 MeV and can be detected through both exclusive and inclusive $\nu_e + {}^{12}\text{C} \rightarrow {}^{12}\text{N} + e^-$ reactions [4]. In the case of ν_μ coming from the decay-in-flight (DIF) of π^+ , the neutrino flux extends on the range (0, 300) MeV, and the $\nu_\mu \rightarrow \nu_e$ appearance mode is looked for experimentally through the reaction $\nu_\mu + {}^{12}\text{C} \rightarrow {}^{12}\text{N} + \mu^-$, which also has been measured [5]. On the other hand we don't have at our disposal experimental information on the ν_e -reaction in the DIF energy range, which is necessary in the evaluation of the oscillation probabilities. Therefore, it is imperative to develop nuclear models, capable of reproducing the ν_e -DAR and ν_μ -DIF data, to be used to predict reliable values for the $\nu_e + {}^{12}\text{C} \rightarrow {}^{12}\text{N} + e^-$ cross section in the DIF energy range, and to calibrate forthwith the $\nu_\mu \rightarrow \nu_e$ appearance probability. Needless to say that, in addition and for consistence, the implemented model also should describe properly the well-known ${}^{12}\text{N} \rightarrow {}^{12}\text{C} + \nu_e + e^+$ β^+ -decay and the $\mu^- + {}^{12}\text{C} \rightarrow \nu_\mu + {}^{12}\text{B}$ muon-capture modes.

The weak interaction formalism most frequently employed in the literature is that of Donnelly and Walecka [6, 7], where the nuclear form factors are classified as Coulomb (\mathcal{M}), longitudinal (\mathcal{L}), transverse electric (\mathcal{T}^{el}) and transverse magnetic (\mathcal{T}^{mag}), in close analogy with the electromagnetic transitions. They in turn depend on seven nuclear matrix elements, denoted as: $M_J^M, \Delta_J^M, \Delta'_J{}^M, \Sigma_J^M, \Sigma'_J{}^M, \Sigma''_J{}^M$, and Ω_J^M . In studying neutrino induced reactions sometimes [8, 9], however, it is preferred to employ the formulation done by Kuramoto *et al.*[10], mainly because of its simplicity. The later formalism does not include the velocity dependent terms in the hadronic current, and therefore the reaction cross section only depends on three nuclear form factors, denoted as $|\langle f|\tilde{1}|i\rangle|^2, |\langle f|\tilde{\sigma}|i\rangle|^2$ and Λ . More,

in applying the formalism of Kuramoto *et al.*[10] for the neutrino-nucleus cross section, it is necessary to recur to other theoretical developments for the muon capture rate, such as those of Luyten *et al.*[11] and Auerbach and Klein [12], where are used the matrix elements M_V^2 , M_A^2 and M_P^2 , which relate to the former ones in a non-trivial way.

Quite recently, we have carried out a multipole expansion of the $V - A$ hadronic current, similar to the one used by Barbero *et al.* [13] for the neutrinoless double beta decay, expressing all above mentioned observables in terms of the vector (V) and axial vector (A) nuclear form factors \mathcal{M}_V and \mathcal{M}_A^M , with $M = -1, 0, +1$ [14]. Such a classification is closely related to the $V - A$ structure of the weak current and to the currently used nuclear β -decay formalisms, where the nuclear moments are expressed in a way that the *forbiddenness* of the transitions is easily recognized. This in no way means that we have developed a new theoretical framework; the final results can be found in one form or another in the literature. The main difference stems from the fact that we use the Racah algebra from the start, employing the spherical spatial coordinates instead of the cartesian ones. Concomitantly, we also express the lepton trace in spherical coordinates, as done for instance in the book of Supek [15]. Here we present a few more details than in Ref. [14] on the procedure which we have followed and also consider the first order nonlocal corrections, which give rise to the additional matrix elements $\mathcal{M}_{V'}^M$ and $\mathcal{M}_{A'}$.

In Ref. [14] we have analyzed the inconveniences that appear in applying RPA like nuclear models for describing the nuclear structure of the $\{^{12}B, ^{12}C, ^{12}N\}$ triad. We have established that the projected quasiparticle RPA (PQRPA) was the proper approach to treat both the short range pairing and the long range RPA correlations. More details are given in the present work, putting special emphasis on the differences between the projected and the usual QRPA approximations. We also compare our PQRPA cross sections with recent shell model (SM) calculations [16, 17], and analyze the reliability of the calculated energy dependence of the $\nu_e + ^{12}C \rightarrow ^{12}N + e^-$ cross-section in the DIF energy region to be used in the evaluation of the oscillation probabilities.

The work will be organized as follows. In Section II we explain our multipole decomposition of the weak current and present the corresponding formula for the neutrino-nucleus cross section and the μ -capture. In Section III we briefly overview the projected BCS (PBCS) and the PQRPA equations. The main reason for the last is to emphasize the relationship with the usual QRPA approximation, which is difficult to find in the existing literature.

Finally, in Section IV we show the numerical results which come from the PQRPA model and compare them with the most recent shell model calculations.

II. FORMALISM FOR THE WEAK INTERACTING PROCESSES

The weak Hamiltonian is expressed in the form [6, 7, 13, 18]

$$H_W(\mathbf{r}) = \frac{G}{\sqrt{2}} J_\alpha l_\alpha e^{-i\mathbf{r}\cdot\mathbf{k}}, \quad (2.1)$$

where $G = (3.04545 \pm 0.00006) \times 10^{-12}$ is the Fermi coupling constant (in natural units),

$$J_\alpha = i\gamma_4 \left[g_V \gamma_\alpha - \frac{g_M}{2M} \sigma_{\alpha\beta} k_\beta + g_A \gamma_\alpha \gamma_5 + i \frac{g_P}{m_\ell} k_\alpha \gamma_5 \right] \equiv (\mathbf{J}, iJ_\emptyset) \quad (2.2)$$

is the hadronic current operator [32], and

$$l_\alpha = -i\bar{u}_{s_\ell}(\mathbf{p}, E_\ell) \gamma_\alpha (1 + \gamma_5) u_{s_\nu}(\mathbf{q}, E_\nu) \equiv (\mathbf{l}, il_\emptyset) \quad (2.3)$$

is the plane waves approximation for the matrix element of the leptonic current in the case of neutrino reactions. Here $\alpha, \beta (= 1, 2, 3, 4)$ and a metric is used in which $x = \{\mathbf{x}, x_4 = ix_\emptyset\}$; we use the index \emptyset for the temporal component, and we reserve the index 0 for the spherical third component. The quantity

$$k = P_i - P_f \equiv \{\mathbf{k}, ik_\emptyset\} \quad (2.4)$$

is the momentum transfer (P_i and P_f are momenta of the initial and final nucleon (nucleus), M is the nucleon mass, m_ℓ is the mass of the charged lepton, and g_V, g_A, g_M and g_P are, respectively, the vector, axial-vector, weak-magnetism and pseudoscalar effective dimensionless coupling constants. Their numerical values are

$$\begin{aligned} g_V &= 1; \quad g_A = 1.26; \\ g_M &= \kappa_p - \kappa_n = 3.70; \quad g_P = g_A \frac{2Mm_\ell}{k^2 + m_\pi^2}. \end{aligned} \quad (2.5)$$

We use here the Walecka's notation [7] with the Euclidean metric for the quadrivectors. The only difference is that we substitute his indices (0, 3) by our indices ($\emptyset, 0$).

The finite nuclear size (FNS) effect is incorporated via the dipole form factor with a cutoff $\Lambda = 850$ MeV, *i.e.*, as:

$$g \rightarrow g \left(\frac{\Lambda^2}{\Lambda^2 + k^2} \right)^2.$$

To use (2.1) with the non-relativistic nuclear wave functions, the Foldy-Wouthuysen transformation has to be performed on the hadronic current (2.2). When the velocity dependent terms are included this yields:

$$\begin{aligned} J_\emptyset &= g_V + (\bar{g}_A + \bar{g}_{P1})\boldsymbol{\sigma} \cdot \hat{\mathbf{k}} - g_A\boldsymbol{\sigma} \cdot \mathbf{v}, \\ \mathbf{J} &= -g_A\boldsymbol{\sigma} - i\bar{g}_W\boldsymbol{\sigma} \times \hat{\mathbf{k}} - \bar{g}_V\hat{\mathbf{k}} + \bar{g}_{P2}(\boldsymbol{\sigma} \cdot \hat{\mathbf{k}})\hat{\mathbf{k}} + g_V\mathbf{v}, \end{aligned} \quad (2.6)$$

where $\mathbf{v} \equiv -i\nabla/M$ is the velocity operator, acting on the nuclear wave functions. The following short notation has been introduced:

$$\begin{aligned} \bar{g}_V &= g_V \frac{\kappa}{2M}; \quad \bar{g}_A = g_A \frac{\kappa}{2M}; \quad \bar{g}_W = (g_V + g_M) \frac{\kappa}{2M}, \\ \bar{g}_{P1} &= g_P \frac{\kappa}{2M} \frac{k_\emptyset}{m_\ell}; \quad \bar{g}_{P2} = g_P \frac{\kappa}{2M} \frac{\kappa}{m_\ell}, \end{aligned} \quad (2.7)$$

where $\kappa \equiv |\mathbf{k}|$.

In performing the multipole expansion of the nuclear operator

$$O_\alpha \equiv (\mathbf{O}, iO_\emptyset) = J_\alpha e^{-i\mathbf{k} \cdot \mathbf{r}}, \quad (2.8)$$

the momentum \mathbf{k} is taken to be along the z axis, *i.e.*,

$$e^{-i\mathbf{k} \cdot \mathbf{r}} = \sum_L i^{-L} \sqrt{4\pi(2L+1)} j_L(\kappa r) Y_{L0}(\hat{\mathbf{r}}), \quad (2.9)$$

and one gets

$$\begin{aligned} O_\emptyset &= \sum_J i^{-J} \sqrt{4\pi(2J+1)} j_J(\kappa r) Y_{J0}(\hat{\mathbf{r}}) J_\emptyset, \\ O_M &= \sum_{JL} i^{-L} F_{JLM} \sqrt{4\pi(2J+1)} j_L(\kappa r) [Y_L(\hat{\mathbf{r}}) \otimes \mathbf{J}]_{JM}. \end{aligned} \quad (2.10)$$

The geometrical factors

$$F_{JLM} \equiv (-)^{J+M} \sqrt{(2L+1)} \begin{pmatrix} L & 1 & J \\ 0 & -M & M \end{pmatrix}, \quad (2.11)$$

which will be seldom used in our work, fulfill the sum rule

$$\sum_L F_{JLM} F_{JLM'} = \delta_{MM'}, \quad (2.12)$$

and their explicit values are listed in Table I.

TABLE I: Values of the geometrical factors F_{JLM} .

M	L	F_{JLM}
0	$J + 1$	$-\sqrt{\frac{J+1}{2J+1}}$
0	J	0
0	$J - 1$	$\sqrt{\frac{J}{2J+1}}$
1	$J + 1$	$\frac{1}{\sqrt{2}}\sqrt{\frac{J}{2J+1}}$
1	J	$-\frac{1}{\sqrt{2}}$
1	$J - 1$	$\frac{1}{\sqrt{2}}\sqrt{\frac{J+1}{2J+1}}$
-1	$J + 1$	$\frac{1}{\sqrt{2}}\sqrt{\frac{J}{2J+1}}$
-1	J	$\frac{1}{\sqrt{2}}$
-1	$J - 1$	$\frac{1}{\sqrt{2}}\sqrt{\frac{J+1}{2J+1}}$

After some Racah algebra we find

$$O_\alpha = \sum_J \sqrt{2J+1} O_\alpha(J), \quad (2.13)$$

with

$$O_\emptyset(J) = i^{-J} \sqrt{4\pi} [g_V Y_{J0}(\kappa \mathbf{r}) - g_A Y_{J0}(\kappa \mathbf{r}, \boldsymbol{\sigma} \cdot \mathbf{v})] + \sqrt{4\pi} (\bar{g}_A + \bar{g}_{P1}) \sum_{L=J\pm 1} i^{-L} F_{JL0} \mathcal{S}_{JL0}(\kappa \mathbf{r}), \quad (2.14)$$

and

$$O_M(J) = \sqrt{4\pi} \sum_L i^{-L} F_{JLM} \left[-g_A \mathcal{S}_{JLM}(\kappa \mathbf{r}) + g_V \mathcal{P}_{JLM}(\kappa \mathbf{r}) - i(-)^J \bar{g}_V F_{JL0} Y_{JM}(\kappa \mathbf{r}) \right. \\ \left. + \sum_I \left(i(-)^L \bar{g}_W G_{JLI} + \bar{g}_{P2} F_{JL0} F_{JI0} \right) \mathcal{S}_{JIM}(\kappa \mathbf{r}) \right], \quad (2.15)$$

where we have introduced the operators listed in Table II, and the coefficients

$$G_{JLI} = (-)^J \sqrt{6(2L+1)(2I+1)} \begin{Bmatrix} 1 & 1 & 1 \\ I & L & J \end{Bmatrix} \begin{pmatrix} I & 1 & L \\ 0 & 0 & 0 \end{pmatrix}, \quad (2.16)$$

TABLE II: Elemental operators and their parities.

Operator	Parity
$\Upsilon_{JM}(\kappa\mathbf{r}) = j_J(\kappa r)Y_{JM}(\hat{\mathbf{r}})$	$(-)^J$
$\mathbf{S}_{JLM}(\kappa\mathbf{r}) = j_L(\kappa r)[Y_L(\hat{\mathbf{r}}) \otimes \boldsymbol{\sigma}]_{JM}$	$(-)^L$
$\mathbf{P}_{JLM}(\kappa\mathbf{r}) = j_L(\kappa r)[Y_L(\hat{\mathbf{r}}) \otimes \mathbf{v}]_{JM}$	$(-)^{L+1}$
$\Upsilon_{JM}(\kappa\mathbf{r}, \boldsymbol{\sigma} \cdot \mathbf{v}) = j_J(\kappa r)Y_{JM}(\hat{\mathbf{r}})(\boldsymbol{\sigma} \cdot \mathbf{v})$	$(-)^{J+1}$

which obey the sum rule

$$\sum_L F_{JLM}G_{JLI} = -MF_{JIM}. \quad (2.17)$$

Using (2.12) and (2.17) we can rewrite the spherical components of $\mathbf{O}_M(J)$ as

$$\begin{aligned} \mathbf{O}_M(J) &= \sqrt{4\pi} \sum_L i^{-L} F_{JLM} \left[(-g_A + M\bar{g}_W + \bar{g}_{P2}\delta_{M0})\mathbf{S}_{JLM}(\kappa\mathbf{r}) + g_V\mathbf{P}_{JLM}(\kappa\mathbf{r}) \right] \\ &\quad - \sqrt{4\pi} i^{-J} \bar{g}_V \delta_{M0} \Upsilon_{J0}(\kappa\mathbf{r}). \end{aligned} \quad (2.18)$$

For the neutrino-nucleus reaction the momentum transfer is $k = p_\ell - q_\nu$, with $p_\ell \equiv \{\mathbf{p}_\ell, iE_\ell\}$ and $q_\nu \equiv \{\mathbf{q}_\nu, iE_\nu\}$, and the corresponding cross section reads

$$\sigma(E_\ell, J_f) = \frac{|\mathbf{p}_\ell|E_\ell}{2\pi} F(Z+1, E_\ell) \int_{-1}^1 d(\cos\theta) \mathcal{T}_\sigma(\kappa, J_f), \quad (2.19)$$

where $F(Z+1, E_\ell)$ is the Fermi function, $\theta \equiv \hat{\mathbf{q}}_\nu \cdot \hat{\mathbf{p}}_\ell$, and

$$\mathcal{T}_\sigma(\kappa, J_f) \equiv \frac{1}{2J_i+1} \sum_{s_\ell, s_\nu} \sum_{M_i, M_f} |\langle J_f M_f | H_W | J_i M_i \rangle|^2, \quad (2.20)$$

with $|J_i M_i\rangle$ and $|J_f M_f\rangle$ being the nuclear initial and final state vectors.

The weak hamiltonian matrix element reads

$$\langle J_f M_f | H_W | J_i M_i \rangle = \frac{G}{\sqrt{2}} \mathcal{O}_\alpha l_\alpha, \quad (2.21)$$

where

$$\mathcal{O}_\alpha \equiv \langle J_f M_f | \mathcal{O}_\alpha | J_i M_i \rangle, \quad (2.22)$$

and l_α is the leptonic current defined in (2.3). Thus

$$\mathcal{T}_\sigma(\kappa, J_f) = \frac{G^2}{2J_i + 1} \sum_{M_i M_f} \mathcal{O}_\alpha \mathcal{O}_\beta^* \mathcal{L}_{\alpha\beta}, \quad (2.23)$$

where, the lepton trace $\mathcal{L}_{\alpha\beta}$, when expressed in cartesian spatial coordinates, reads

$$\mathcal{L}_{\alpha\beta} = \frac{1}{2} \sum_{s_\ell s_\nu} l_\alpha l_\beta^* = -\frac{1}{E_\ell E_\nu} [p_\alpha q_\beta + q_\alpha p_\beta - \delta_{\alpha\beta}(\mathbf{p} \cdot \mathbf{q}) \pm \epsilon_{\alpha\beta\gamma\delta} q_\gamma p_\delta], \quad (2.24)$$

the positive (negative) sign standing for neutrino (antineutrino) scattering.

It is convenient to follow Ref. [15] and express the spatial parts of \mathcal{O} and \mathcal{L} in spherical coordinates ($M, M' = 0, -1, 1$). In this way one might write

$$\mathcal{T}_\sigma(\kappa, J_f) = \frac{G^2}{2J_i + 1} \sum_{M_f M_i} \left[|\mathcal{O}_\emptyset|^2 \mathcal{L}_{\emptyset\emptyset} + \sum_{MM'} \mathcal{O}_M \mathcal{O}_{M'}^* \mathcal{L}_{MM'} - 2\Re \left(\mathcal{O}_\emptyset^* \sum_M (-)^M \mathcal{O}_{-M} \mathcal{L}_{\emptyset M} \right) \right], \quad (2.25)$$

with [15]

$$\mathcal{L}_{\emptyset\emptyset} \equiv \mathcal{L}_{44} = 1 + \frac{\mathbf{p} \cdot \mathbf{q}}{E_\ell E_\nu}, \quad (2.26)$$

$$\mathcal{L}_{\emptyset M} \equiv -i\mathcal{L}_{4M} = \frac{1}{E_\ell E_\nu} [E_\ell q_M + E_\nu p_M \mp i(\mathbf{q} \times \mathbf{p})_M], \quad (2.27)$$

$$\begin{aligned} \mathcal{L}_{MM'} &= \delta_{MM'} + \frac{1}{E_\ell E_\nu} (q_M^* p_{M'} + q_{M'} p_M^* - \delta_{MM'} \mathbf{p} \cdot \mathbf{q}) \\ &\pm \sqrt{6} \sum_m (-)^{M'+m} \begin{pmatrix} 1 & 1 & 1 \\ -M & M' & m \end{pmatrix} \left(\frac{q_m^*}{E_\nu} - \frac{p_m^*}{E_\ell} \right). \end{aligned} \quad (2.28)$$

From the Wigner-Eckart theorem we also get:

$$\mathcal{O}_\emptyset = \sum_J (-)^{J_f - M_f} \sqrt{2J + 1} \begin{pmatrix} J_f & J & J_i \\ -M_f & 0 & M_i \end{pmatrix} \langle J_f || \mathbf{O}_\emptyset(J) || J_i \rangle, \quad (2.29)$$

and

$$\mathcal{O}_M = \sum_J (-)^{J_f - M_f} \sqrt{2J + 1} \begin{pmatrix} J_f & J & J_i \\ -M_f & M & M_i \end{pmatrix} \langle J_f || \mathbf{O}_M(J) || J_i \rangle. \quad (2.30)$$

Using now the orthogonality condition

$$\sum_{M_i M_f} \begin{pmatrix} J_f & J & J_i \\ -M_f & M & M_i \end{pmatrix} \begin{pmatrix} J_f & J' & J_i \\ -M_f & M' & M_i \end{pmatrix} = \frac{1}{(2J + 1)} \delta_{JJ'} \delta_{MM'} \quad (2.31)$$

one obtains

$$\mathcal{T}_\sigma(\kappa, J_f) = \frac{G^2}{2J_i + 1} \sum_J \left[|\langle J_f || \mathbf{O}_\emptyset(J) || J_i \rangle|^2 \mathcal{L}_{\emptyset\emptyset} + \sum_M |\langle J_f || \mathbf{O}_M(J) || J_i \rangle|^2 \mathcal{L}_{MM} - 2\Re(\langle J_f || \mathbf{O}_\emptyset(J) || J_i \rangle^* \langle J_f || \mathbf{O}_0(J) || J_i \rangle \mathcal{L}_{\emptyset 0}) \right], \quad (2.32)$$

where, from (2.14) and (2.18),

$$\begin{aligned} \langle J_f || \mathbf{O}_\emptyset(J) || J_i \rangle &= \sqrt{2J_i + 1} \left[g_V \mathcal{M}_V(J) - g_A \mathcal{M}_{A'}(J) + (\bar{g}_A + \bar{g}_{P1}) \mathcal{M}_A^0(J) \right] \\ \langle J_f || \mathbf{O}_M(J) || J_i \rangle &= \sqrt{2J_i + 1} \left[(-g_A + M\bar{g}_W + \bar{g}_{P2}\delta_{M0}) \mathcal{M}_A^M(J) + g_V \mathcal{M}_{V'}^M(J) - \bar{g}_V \delta_{M0} \mathcal{M}_V(J) \right], \end{aligned} \quad (2.33)$$

with the nuclear matrix elements defined as

$$\begin{aligned} \mathcal{M}_V(J) &= i^{-J} \sqrt{\frac{4\pi}{2J_i + 1}} \langle J_f || \mathbf{Y}_J(\kappa \mathbf{r}) || J_i \rangle, \\ \mathcal{M}_A^M(J) &= \sqrt{\frac{4\pi}{2J_i + 1}} \sum_L i^{-L} F_{JLM} \langle J_f || \mathbf{S}_{JL}(\kappa \mathbf{r}) || J_i \rangle, \\ \mathcal{M}_{A'}(J) &= i^{-J} \sqrt{\frac{4\pi}{2J_i + 1}} \langle J_f || \mathbf{Y}_J(\kappa \mathbf{r}, \boldsymbol{\sigma} \cdot \mathbf{v}) || J_i \rangle, \\ \mathcal{M}_{V'}^M(J) &= \sqrt{\frac{4\pi}{2J_i + 1}} \sum_L i^{-L} F_{JLM} \langle J_f || \mathbf{P}_{JL}(\kappa \mathbf{r}) || J_i \rangle. \end{aligned} \quad (2.34)$$

The explicit expressions for $\mathcal{L}_{\emptyset M}$ and $\mathcal{L}_{MM'}$ that appear in (2.32) are [14]:

$$\begin{aligned} \mathcal{L}_{\emptyset\emptyset} &= \left(\frac{q_0}{E_\nu} + \frac{p_0}{E_\ell} \right), \\ \mathcal{L}_{00} &= 1 + \frac{2q_0 p_0 - \mathbf{p} \cdot \mathbf{q}}{E_\ell E_\nu}, \\ \mathcal{L}_{\pm 1, \pm 1} &= 1 - \frac{q_0 p_0}{E_\ell E_\nu} \pm \left(\frac{q_0}{E_\nu} - \frac{p_0}{E_\ell} \right), \end{aligned} \quad (2.35)$$

with

$$\begin{aligned} q_0 &= \hat{k} \cdot \mathbf{q} = \frac{E_\nu (|\mathbf{p}| \cos \theta - E_\nu)}{\kappa}, \\ p_0 &= \hat{k} \cdot \mathbf{p} = \frac{|\mathbf{p}| (|\mathbf{p}| - E_\nu \cos \theta)}{\kappa}. \end{aligned} \quad (2.36)$$

Finally, the transition amplitude can be cast in the form:

$$\begin{aligned} \mathcal{T}_\sigma(\kappa, J_f) &= G^2 \sum_J \left\{ \mathcal{L}_{\emptyset\emptyset} \left[g_V^2 |\mathcal{M}_V(J)|^2 + |(\bar{g}_A + \bar{g}_{P1}) \mathcal{M}_A^0(J) - g_A \mathcal{M}_{A'}(J)|^2 \right] \right. \\ &\quad \left. + \mathcal{L}_{00} \left[\Re \left[(\bar{g}_V \mathcal{M}_V(J) - 2g_V \mathcal{M}_{V'}^0(J)) \bar{g}_V \mathcal{M}_V^*(J) \right] + (\bar{g}_{P2}^2 - 2g_A \bar{g}_{P2}) |\mathcal{M}_A^0(J)|^2 \right] \right\} \end{aligned}$$

$$\begin{aligned}
& + \sum_{M=0,\pm 1} \mathcal{L}_{MM} \left| (g_A - M\bar{g}_W) \mathcal{M}_A^M(J) - g_V \mathcal{M}_{V'}^M(J) \right|^2 \\
& + 2\mathcal{L}_{\emptyset 0} \Re \left(g_V \left[\bar{g}_V \mathcal{M}_V(J) - g_V \mathcal{M}_{V'}^0(J) \right] \mathcal{M}_V^*(J) \right. \\
& \quad \left. + (g_A - \bar{g}_{P_2}) \left[(\bar{g}_A + \bar{g}_{P_1}) \mathcal{M}_A^0(J) - g_A \mathcal{M}_{A'}(J) \right] \mathcal{M}_A^{0*}(J) \right) \Big\}. \tag{2.37}
\end{aligned}$$

The muon capture transition amplitude $\mathcal{T}_\Lambda(J_f)$ can be derived from the result (2.32) for the neutrino-nucleus reaction amplitude, by keeping in mind that: i) the roles of p and q are interchanged within the matrix element of the leptonic current, which brings in a minus sign in the last term of $\mathcal{L}_{\pm 1, \pm 1}$, ii) the momentum transfer turns out to be $k = q - p$, and therefore the signs of the right-hand sides of (2.36) have to be changed, and iii) the threshold values ($\mathbf{p} \rightarrow 0 : \mathbf{k} \rightarrow \mathbf{q}, k_\emptyset \rightarrow E_\nu - m_\ell$) must be used for the lepton traces. All this yields:

$$\mathcal{L}_{\emptyset\emptyset} = \mathcal{L}_{00} = \mathcal{L}_{\emptyset 0} = 1, \quad \mathcal{L}_{\pm 1, \pm 1} = 1 \mp 1. \tag{2.38}$$

One should also remember that instead of summing over the initial lepton spins s_ℓ , as done in (2.20), one has now to average on the same quantum number, getting

$$\Lambda(J_f) = \frac{E_\nu^2}{2\pi} |\phi_{1S}|^2 \mathcal{T}_\Lambda(J_f), \tag{2.39}$$

where ϕ_{1S} is the muonic bound state wave function evaluated at the origin, and $E_\nu = m_\mu - (M_n - M_p) - E_B^\mu - E_f + E_i$, where E_B^μ is the binding energy of the muon in the 1S orbit. In view of (2.39) the transition amplitude reads:

$$\mathcal{T}_\Lambda(J_f) = \frac{G^2}{2J_i + 1} \sum_J \left[|\langle J_f || \mathbf{O}_\emptyset(J) - \mathbf{O}_0(J) || J_i \rangle|^2 + 2|\langle J_f || \mathbf{O}_{-1}(J) || J_i \rangle|^2 \right], \tag{2.40}$$

which, based on the parity considerations, can be expressed as

$$\begin{aligned}
\mathcal{T}_\Lambda(J_f) = G^2 \sum_J \Big\{ & \left| (g_V + \bar{g}_V) \mathcal{M}_V(J) - g_V \mathcal{M}_{V'}^0(J) \right|^2 + \left| (g_A + \bar{g}_A - \bar{g}_P) \mathcal{M}_A^0(J) - g_A \mathcal{M}_{A'}(J) \right|^2 \\
& + 2 \left| (g_A + \bar{g}_W) \mathcal{M}_A^{-1}(J) - g_V \mathcal{M}_{V'}^{-1}(J) \right|^2 \Big\}, \tag{2.41}
\end{aligned}$$

where $\bar{g}_P = \bar{g}_{P_2} - \bar{g}_{P_1}$. In the case of muon capture, it is convenient to rewrite the effective coupling constants as [11]

$$\begin{aligned}
\bar{g}_V &= g_V \frac{E_\nu}{2M}; \quad \bar{g}_A = g_A \frac{E_\nu}{2M}; \\
\bar{g}_W &= (g_V + g_M) \frac{E_\nu}{2M}; \quad \bar{g}_{P_1} = g_P \frac{E_\nu}{2M}. \tag{2.42}
\end{aligned}$$

Lastly, we mention that the B -values for the Gamow-Teller (GT) beta transitions are defined and related to the ft -values as [19]:

$$\frac{|g_A \langle J_f || \sigma || J_i \rangle|^2}{2J_i + 1} \equiv B(GT) = \frac{6146}{ft} \text{ sec.} \quad (2.43)$$

Let us now compare our matrix elements with those currently used in the literature. First, in the Walecka's notation (see Eqs. (45.13) in Ref. [7]) one has

$$\begin{aligned} \mathcal{O}_0(J) &= \mathcal{M}_{J0}, \\ \mathcal{O}_M(J) &= \begin{cases} \mathcal{L}_{J0}, & \text{for } M = 0, \\ -\frac{1}{\sqrt{2}} [M\mathcal{T}_{JM}^{mag} + \mathcal{T}_{JM}^{el}], & \text{for } M = \pm 1, \end{cases} \end{aligned} \quad (2.44)$$

where the meaning of \mathcal{M}_{J0} and \mathcal{L}_{J0} is self evident, while

$$\begin{aligned} \mathcal{T}_{JM}^{el} &= \bar{g}_w \mathcal{S}_{JJM} - i^J \sqrt{2} \sum_{L=J\pm 1} i^{-L} F_{JLM} \left[g_A \mathcal{S}_{JLM} - g_V \mathcal{P}_{JLM} \right], \\ \mathcal{T}_{JM}^{mag} &= -g_A \mathcal{S}_{JJM} + g_V \mathcal{P}_{JJM} + i^J \sqrt{2} \bar{g}_w \sum_{L=J\pm 1} i^{-L} F_{JLM} \mathcal{S}_{JLM}. \end{aligned} \quad (2.45)$$

The matrix elements defined by Donelly [6] are related to ours as:

$$\begin{aligned} M_J^M(\kappa \mathbf{r}) &= Y_{JM}(\kappa \mathbf{r}), \\ \Delta_J^M(\kappa \mathbf{r}) &= \left(\frac{iM}{\kappa} \right) \mathcal{P}_{JJM}(\kappa \mathbf{r}), \\ \Delta_J^{\prime M}(\kappa \mathbf{r}) &= i^J \sqrt{2} \left(\frac{M}{\kappa} \right) \sum_{L=J\pm 1} i^{-L} F_{JLM} \mathcal{P}_{LJM}(\kappa \mathbf{r}), \\ \Sigma_J^M(\kappa \mathbf{r}) &= \mathcal{S}_{JJM}(\kappa \mathbf{r}), \\ \Sigma_J^{\prime M}(\kappa \mathbf{r}) &= i^{J-1} \sqrt{2} \sum_{L=J\pm 1} i^{-L} F_{JLM} \mathcal{S}_{JLM}(\kappa \mathbf{r}), \\ \Sigma_J^{\prime\prime M}(\kappa \mathbf{r}) &= i^{J-1} \sum_{L=J\pm 1} i^{-L} F_{JL0} \mathcal{S}_{JLM}(\kappa \mathbf{r}), \\ \Omega_J^M(\kappa \mathbf{r}) &= \left(\frac{iM}{\kappa} \right) Y_{JM}(\kappa \mathbf{r}, \boldsymbol{\sigma} \cdot \mathbf{v}). \end{aligned} \quad (2.46)$$

The relationship between our formalism and those from Refs. [10, 11] can be obtained from the formula

$$\begin{aligned} \begin{pmatrix} L & 1 & J \\ 0 & M & -M \end{pmatrix} \begin{pmatrix} L' & 1 & J \\ 0 & M & -M \end{pmatrix} &= \frac{\delta_{LL'}}{3(2L+1)} - M \sqrt{\frac{3}{2}} \begin{pmatrix} L & L' & 1 \\ 0 & 0 & 0 \end{pmatrix} \begin{Bmatrix} L & 1 & J \\ 1 & L' & 1 \end{Bmatrix} \\ &+ (-)^{J+1} \sqrt{\frac{5}{6}} (3M^2 - 2) \begin{pmatrix} L & L' & 2 \\ 0 & 0 & 0 \end{pmatrix} \begin{Bmatrix} L & 1 & J \\ 1 & L' & 2 \end{Bmatrix}. \end{aligned} \quad (2.47)$$

For the matrix elements of Kuramoto *et al.*[10] we get

$$\begin{aligned}
|\langle f|\tilde{1}|i\rangle|^2 &= \sum_J |\mathcal{M}_V(J)|^2, \\
\langle f|\tilde{\sigma}|i\rangle|^2 &= \sum_J \sum_{M=0,\pm 1} |\mathcal{M}_A^M(J)|^2, \\
\Lambda &= \frac{1}{3} \sum_J (|\mathcal{M}_A^0(J)|^2 - |\mathcal{M}_A^1(J)|^2);
\end{aligned} \tag{2.48}$$

and for those of Luyten *et al.*[11]

$$\begin{aligned}
M_V^2 &= \left(\frac{E_\nu}{m_\mu}\right)^2 \sum_J |\mathcal{M}_V(J)|^2, \\
M_A^2 &= \left(\frac{E_\nu}{m_\mu}\right)^2 \sum_J \sum_{M=0,\pm 1} |\mathcal{M}_A^M(J)|^2, \\
M_P^2 &= \left(\frac{E_\nu}{m_\mu}\right)^2 \sum_J |\mathcal{M}_A^0(J)|^2.
\end{aligned} \tag{2.49}$$

III. PROJECTED QRPA FORMALISM

We have shown in Ref. [14] that to account for the weak decay observables in a light $N = Z$ nucleus in the framework of the RPA, besides including the BCS correlations, it is imperative to perform the particle number projection. This is an important difference when compared with the treatment of the charge-exchange excitations in heavy nuclei, where very seldom the neutron excess is large and as a consequence the projection procedure is not crucial [20]. In this section we give a more detailed overview of the projected BCS (PBCS) and projected QRPA (PQRPA) approximations.

When the the excited states $|J_f\rangle$ in the final ($Z \pm 1, N \mp 1$) nuclei are described within the PQRPA, the transition amplitudes for the multipole charge-exchange operators Υ_J , *etc.*, listed in Table II, read

$$\begin{aligned}
\langle J_f, Z + \mu, N - \mu | \Upsilon_J | 0^+ \rangle &= \frac{1}{(IZI^N)^{1/2}} \sum_{pn} \left[\frac{\Lambda_\mu(pnJ)}{(I^{Z-1+\mu}(p)I^{N-1+\mu}(n))^{1/2}} X_\mu^*(pnJ_f) \right. \\
&\quad \left. + \frac{\Lambda_{-\mu}(pnJ)}{(I^{Z-1-\mu}(p)I^{N-1-\mu}(n))^{1/2}} Y_\mu^*(pnJ_f) \right],
\end{aligned} \tag{3.1}$$

with the one-body matrix elements given by

$$\Lambda_\mu(pnJ) = -\frac{\langle p | \Upsilon_J | n \rangle}{\sqrt{2J+1}} \begin{cases} u_p v_n, & \text{for } \mu = +1 \\ u_n v_p, & \text{for } \mu = -1 \end{cases}, \tag{3.2}$$

where

$$I^K(k_1 k_2 \cdots k_n) = \frac{1}{2\pi i} \oint \frac{dz}{z^{K+1}} \sigma_{k_1} \cdots \sigma_{k_n} \prod_k (u_k^2 + z^2 v_k^2)^{j_k+1/2}; \quad \sigma_k^{-1} = u_k^2 + z_k^2 v_k^2, \quad (3.3)$$

are the PBCS number projection integrals.

The PBCS gap equations are

$$2\bar{e}_k u_k v_k - \Delta_k (u_k^2 - v_k^2) = 0, \quad (3.4)$$

where

$$\Delta_k = -\frac{1}{2} \sum_{k'} \frac{(2j_{k'} + 1)^{1/2}}{(2j_k + 1)^{1/2}} u_{p'} v_{p'} G(k k k' k'; 0) \frac{I^{Z-2}(k k')}{I^Z} \quad (3.5)$$

are the pairing gaps, and

$$\bar{e}_k = e_k \frac{I^{Z-2}(k)}{I^Z} + \sum_{k'} \frac{(2j_{k'} + 1)^{1/2}}{(2j_k + 1)^{1/2}} v_{k'}^2 F(k k k' k'; 0) \frac{I^{Z-4}(k k')}{I^Z} + \Delta e_k, \quad (3.6)$$

are the dressed single-particle energies. The PBCS correction term Δe_k can be found in Ref. [20], and F and G stand for the usual particle-hole (ph) and particle-particle (pp) matrix elements, respectively.

The forward, X_μ , and backward, Y_μ , PQRPA amplitudes are obtained by solving the RPA equations

$$\begin{pmatrix} A_\mu & B \\ -B^* & -A_{-\mu}^* \end{pmatrix} \begin{pmatrix} X_\mu \\ Y_\mu \end{pmatrix} = \omega_\mu \begin{pmatrix} X_\mu \\ Y_\mu \end{pmatrix}, \quad (3.7)$$

with the PQRPA matrices defined as:

$$\begin{aligned} A_\mu(pn, p'n'; J) &= (\varepsilon_p^{Z-1+\mu} + \varepsilon_n^{N-1-\mu}) \delta_{pn, p'n'} + N_\mu(pn)^{-1/2} N_\mu(p'n')^{-1/2} \\ &\times \left\{ [u_p u_n u_{p'} v_{n'} I^{Z-1+\mu}(pp') I^{N-3+\mu}(nn') + v_p u_n v_{p'} u_{n'} I^{Z-3+\mu}(pp') I^{N-1+\mu}(nn')] F(pn, pn; J) \right. \\ &+ [u_p u_n u_{p'} u_{n'} I^{Z-1+\mu}(pp') I^{N-1+\mu}(nn') + v_p v_n v_{p'} v_{n'} I^{Z-3+\mu}(pp') I^{N-3+\mu}(nn')] G(pn, pn; J) \left. \right\}, \\ B(pn, p'n'; J) &= N_\mu(pn)^{-1/2} N_{-\mu}(p'n')^{-1/2} I^{Z-2}(pp') I^{N-2}(nn') \\ &\times [(v_p u_n u_{p'} v_{n'} + u_p v_n v_{p'} u_{n'}) F(pn, pn; J) + (u_p u_n v_{p'} v_{n'} + v_p v_n u_{p'} u_{n'}) G(pn, pn; J)], \quad (3.8) \end{aligned}$$

where

$$N_\mu(pn) = I^{Z-1+\mu}(p) I^{N-1+\mu}(n), \quad (3.9)$$

are the norms,

$$\varepsilon_k^K = \frac{R_0^K(k) + R_{11}^K(kk)}{I^K(k)} - \frac{R_0^K}{I^K} \quad (3.10)$$

are the projected quasiparticle energies, and the quantities R^K are defined as [20]

$$\begin{aligned} R_0^K(k) &= \sum_{k_1} (2j_{k_1} + 1) v_{k_1}^2 e_{k_1} I^{K-2}(kk_1) + \frac{1}{4} \sum_{k_1 k_2} (2j_{k_1} + 1)^{1/2} (2j_{k_2} + 1)^{1/2} \\ &\times \left[v_{k_1}^2 v_{k_2}^2 F(k_1 k_1 k_2 k_2; 0) I^{K-4}(k_1 k_2 k) + u_{k_1} v_{k_1} u_{k_2} v_{k_2} G(k_1 k_1 k_2 k_2; 0) I^{K-2}(k_1 k_2 k) \right], \\ R_{11}^K(kk) &= e_k [u_k^2 I^{k_1}(kk) - v_k^2 I^{K-2}(kk)] + \sum_{k_1} \frac{(2j_{k_1} + 1)^{1/2}}{(2j_k + 1)^{1/2}} \\ &\times \left\{ v_{k_1}^2 F(k_1 k_1 k k; 0) [u_k^2 I^{K-2}(k_1 k k) - v_k^2 I^{K-4}(k_1 k k)] - u_{k_1} v_{k_1} u_k v_k G(k_1 k_1 k k; 0) I^{K-2}(k_1 k k) \right\}. \end{aligned} \quad (3.11)$$

It is worth to note that the PQRPA formalism is valid not only for the particle-hole charge-exchange excitations ($Z \pm 1, N \mp 1$), but also for the charge-exchange pairing-vibrations ($Z \pm 1, N \pm 1$). In the later case one has simply to do the replacement $\mu \rightarrow -\mu$ in the neutron sector.

The usual gap equations are obtained from the Eqs. (3.4)-(3.6) by: 1) the replacement $e_k \rightarrow e_k - \lambda_k$, with λ_k being the chemical potential, 2) going to the limit $I^K \rightarrow 1$, and 3) imposing the subsidiary conditions

$$Z = \sum_{j_p} (2j_p + 1)^2 v_{j_p}^2, \quad N = \sum_{j_n} (2j_n + 1)^2 v_{j_n}^2, \quad (3.12)$$

as the number of particles is not any more a good quantum number.

Finally, the plain QRPA equations are recovered from (3.7) and (3.8) by: 1) dropping the index μ and taking the limit $I^K \rightarrow 1$, and 2) substituting the unperturbed PBCS energies by the BCS energies relative to the Fermi level, *i.e.*, by

$$E_k^{(\pm)} = \pm E_k + \lambda_k, \quad (3.13)$$

where $E_k = ((e_k - \lambda_k)^2 + \Delta_k^2)^{1/2}$ are the usual BCS quasiparticle energies. In this way the the unperturbed energies in (3.8) are replaced as [33]

$$\varepsilon_{j_p}^{Z-1+\mu} + \varepsilon_{j_n}^{N-1-\mu} \rightarrow E_{j_p} + E_{j_n} + \mu(\lambda_p - \lambda_n). \quad (3.14)$$

IV. NUMERICAL RESULTS AND DISCUSSION

In this section, our theoretical results within the PQRPA are confronted with the experimental data for the $\mu^- + {}^{12}\text{B} \rightarrow {}^{12}\text{C} + \nu_\mu$ muon capture rates, as well as for the neutrino cross sections involving the DAR reaction $\nu_e + {}^{12}\text{C} \rightarrow {}^{12}\text{N} + e^-$ and DIF reaction $\nu_\mu + {}^{12}\text{C} \rightarrow {}^{12}\text{N} + \mu^-$. We also exhibit our predictions for the $\nu_e + {}^{12}\text{C} \rightarrow {}^{12}\text{N} + e^-$ differential cross section for ν_e -energies in the DIF energy range. At variance with our previous work, we consider here also the velocity dependent matrix elements $\mathcal{M}_{A'}(J)$ and $\mathcal{M}_{A'}^M(J)$, defined in (2.34).

TABLE III: BCS and PBCS results for neutrons. E_j^{exp} stand for the experimental energies used in the fitting procedure, and e_j are the resulting s.p.e. The underlined quasiparticle energies correspond to single-hole excitations (for $j = 1s_{1/2}, 1p_{3/2}$) and to single-particle excitations (for $j = 1p_{1/2}, 1d_{5/2}, 2s_{1/2}, 1d_{3/2}, 1f_{7/2}, 2p_{3/2}$). The non-underlined energies are mostly two hole-one particle and two particle-one hole excitations. The fitted values of the pairing strengths v_s^{pair} in units of MeV-fm³ are also displayed.

<i>Shell</i>	E_j^{exp}	<i>BCS</i>			<i>PBCS</i>		
		$E_j^{(+)}$	$E_j^{(-)}$	e_j	ϵ_j^N	$-\epsilon_j^{N-2}$	e_j
$1s_{1/2}$		11.34	<u>-35.13</u>	-23.58	19.93	<u>-34.99</u>	-22.37
$1p_{3/2}$	-18.72	-5.07	<u>-18.72</u>	-7.80	-1.28	<u>-18.73</u>	-7.24
$1p_{1/2}$	-4.94	<u>-4.94</u>	-18.85	-2.07	<u>-4.95</u>	-22.33	-1.51
$1d_{5/2}$	-1.09	<u>-1.09</u>	-22.70	2.12	<u>-1.09</u>	-26.82	2.16
$2s_{1/2}$	-1.85	<u>-1.86</u>	-21.93	2.70	<u>-1.85</u>	-25.98	2.68
$1d_{3/2}$	2.72	<u>2.72</u>	-26.51	6.24	<u>2.73</u>	-30.79	6.26
$1f_{7/2}$	5.81	<u>5.82</u>	-29.61	8.14	<u>5.83</u>	-33.61	8.17
$2p_{3/2}$	7.17	<u>7.18</u>	-30.98	11.49	<u>7.16</u>	-35.23	11.47
$2p_{1/2}$		<u>12.89</u>	-36.69	17.30	<u>12.89</u>	-41.01	17.32
$1f_{5/2}$		<u>16.72</u>	-40.52	19.18	<u>16.72</u>	-44.58	19.21
v_s^{pair}				23.16			23.92

The calculations shown here were done in the same way as in the previous work [14]. That

is, for the residual interaction we adopted the delta force,

$$V = -4\pi (v_s P_s + v_t P_t) \delta(r), \quad (4.1)$$

which has been used extensively in the literature [21, 22, 23] for describing the single and double beta decays. The configuration space includes the single-particle orbitals with $nl = (1s, 1p, 1d, 2s, 1f, 2p)$ for both protons and neutrons.

TABLE IV: Same as Table III but for protons.

Shell	E_j^{exp}	<i>BCS</i>			<i>PBCS</i>		
		$E_j^{(+)}$	$E_j^{(-)}$	e_j	ε_j^Z	$-\varepsilon_j^{Z-2}$	e_j
$1s_{1/2}$	-33.00 [†]	14.94	<u>-33.13</u>	-21.62	19.44	<u>-32.99</u>	-20.41
$1p_{3/2}$	-15.95	-2.24	<u>-15.96</u>	-4.95	1.46	<u>-15.95</u>	-4.40
$1p_{1/2}$	-1.94	<u>-1.95</u>	-16.25	1.01	<u>-1.95</u>	-19.76	1.56
$1d_{5/2}$	1.61	<u>1.61</u>	-19.80	4.76	<u>1.61</u>	-23.90	4.83
$2s_{1/2}$	0.42	<u>0.42</u>	-18.61	4.88	<u>0.42</u>	-22.59	4.88
$1d_{3/2}$	4.95	<u>4.95</u>	-23.14	8.40	<u>4.95</u>	-27.37	8.43
$1f_{7/2}$	8.42	<u>8.42</u>	-26.61	10.72	<u>8.42</u>	-30.58	10.75
$2p_{3/2}$	9.76	<u>9.77</u>	-27.96	14.05	<u>9.77</u>	-32.22	14.07
$2p_{1/2}$	16.23	<u>16.23</u>	-34.43	20.63	<u>16.22</u>	-38.73	20.66
$1f_{5/2}$	19.71	<u>19.70</u>	-37.90	22.15	<u>19.71</u>	-41.96	22.20
v_s^{pair}				23.13			23.92
[†] The energy $E_{1s_{1/2}}^{\text{exp}}$ was estimated from a harmonic oscillator well.							

The procedure to fix self-consistently in Eqs. (3.5) and (3.6) both the bare single-particle energies (s.p.e.) e_{j_p} and e_{j_n} , and the corresponding pairing coupling constants $v_s^{\text{pair}}(p)$ and $v_s^{\text{pair}}(n)$, from the experimental energies of the odd-mass nuclei ^{11}C , ^{11}B , ^{13}C and ^{13}N , has been described in detail in Ref. [14]. Here we just show the final results, for neutrons in Table III and for protons in Table IV. It is worth noting that within the PBCS the neutron-energy $\varepsilon_{1p_{3/2}}^N = -1.28$ MeV and the proton-energy $\varepsilon_{1p_{3/2}}^P = 1.46$ MeV nicely agree, respectively, with the experimental energies $E_{3/2_1^-} = -1.26$ MeV in ^{13}C and $E_{3/2_1^-} = 1.55$

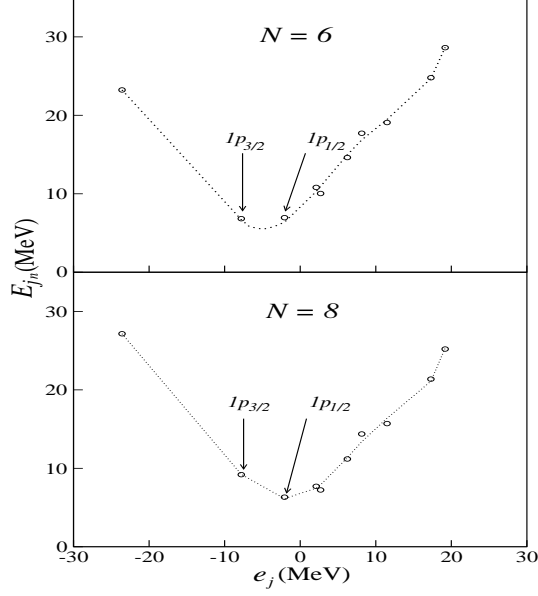


FIG. 1: Neutron quasiparticle excitation energies for $N = 6$ and $N = 8$. The states are ordered as $1s_{1/2}$, $1p_{3/2}$, $1p_{1/2}$, $2s_{1/2}$, $1d_{3/2}$, $1f_{7/2}$, $2p_{3/2}$, $2p_{1/2}$, and $1f_{7/2}$, and the energies are indicated by circles.

MeV in ^{13}N [24]. This does not happen in the BCS case where $E_{1p_{3/2}}^{(+)} = -5.07$ MeV for neutrons and $E_{1p_{3/2}}^{(+)} = -2.44$ MeV for protons.

Before proceeding let us remember an important issue in the description of the $N \cong Z$ nuclei within the QRPA, which is more inherent to the model itself than to the occasional parameterization that might be employed. In fact, a few years ago Volpe *et al.*[9] have called attention on the inconveniences in applying the QRPA to ^{12}N , since the lowest state turned out not to be the most collective one. Later on we have shown [14] that the origin of this difficulty was the degeneracy among the four lowest proton-neutron two-quasiparticle states $|1p_{1/2}1p_{3/2}\rangle$, $|1p_{3/2}1p_{3/2}\rangle$, $|1p_{1/2}1p_{1/2}\rangle$ and $|1p_{3/2}1p_{1/2}\rangle$. It also has been shown in Ref. [14] that it is imperative to use the projected QRPA for a physically sound description of the weak processes among the ground states of the triad $\{^{12}\text{B}, ^{12}\text{C}, ^{12}\text{N}\}$. In fact, when the Fermi level is fixed at $N = Z = 6$, their BCS energies

$$\mathcal{E}_{j_p j_n} = \begin{cases} E_{j_p}^{(+)} - E_{j_n}^{(-)} = E_{j_p} + E_{j_n} + \lambda_p - \lambda_n; & \text{for } ^{12}\text{N}, \\ -E_{j_p}^{(-)} + E_{j_n}^{(+)} = E_{j_p} + E_{j_n} - \lambda_p + \lambda_n; & \text{for } ^{12}\text{B}, \\ E_{j_p}^{(+)} + E_{j_n}^{(+)} = E_{j_p} + E_{j_n} + \lambda_p + \lambda_n; & \text{for } ^{14}\text{N}, \\ -E_{j_p}^{(-)} - E_{j_n}^{(-)} = E_{j_p} + E_{j_n} - \lambda_p - \lambda_n; & \text{for } ^{10}\text{B}, \end{cases} \quad (4.2)$$

are almost degenerate for all four odd-odd ($Z \pm 1, N \mp 1$) and ($Z \pm 1, N \pm 1$) nuclei. As illustrated in Fig. 1, this, in turn, comes from the fact that for $N = Z = 6$ the quasiparticle energies $E_{1p_{1/2}}$ and $E_{1p_{3/2}}$ are very close to each other. In the upper panel of Fig. 2 are shown the BCS energies (4.2), as a function of N , of the just mentioned four states in the case of nitrogen isotopes. One notices that for $N \neq Z$ the degeneracy is removed yet only partially. But, as seen from the lower panel in Fig. 2, the degeneracy discussed above is totally removed when the number projection is done.

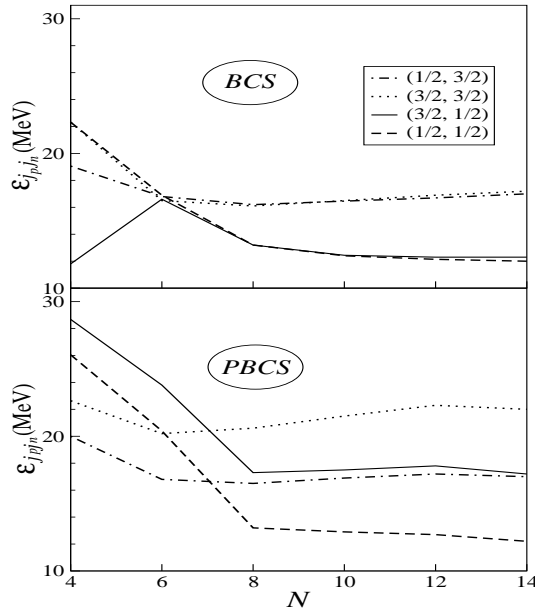


FIG. 2: Unperturbed two-quasiparticle energies $\mathcal{E}_{j_p j_n}$ for nitrogen isotopes, as a function of N , of the states $|1p_{1/2}1p_{3/2}\rangle$, $|1p_{3/2}1p_{3/2}\rangle$, $|1p_{1/2}1p_{1/2}\rangle$ and $|1p_{3/2}1p_{1/2}\rangle$. In the upper (lower) panel are shown the BCS (PBCS) results.

More, within the PBCS in the case of ^{12}N , for instance, we get from numerical calculations

$$\begin{aligned} \mathcal{E}_{1p_{3/2}1p_{3/2}} &\cong \mathcal{E}_{1p_{1/2}1p_{1/2}} \cong \mathcal{E}_{1p_{1/2}1p_{3/2}} + \Delta, \\ \mathcal{E}_{1p_{3/2}1p_{1/2}} &\cong \mathcal{E}_{1p_{1/2}1p_{3/2}} + 2\Delta, \end{aligned} \quad (4.3)$$

with $\Delta = 3.4$ MeV. The meaning of this results can be easily disentangled by referring to the shell-model and analyzing the particle-hole (ph) limits of the proton-neutron two-quasiparticle states, which are pictorially shown in Fig. 3. One sees that, while $|1p_{1/2}1p_{3/2}\rangle$

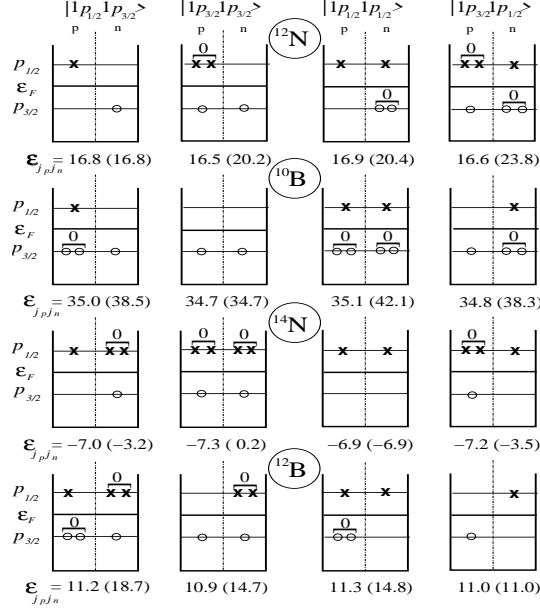


FIG. 3: Schematic representation of the particle-hole limits for the seniority-two pn-states. The zero-angular-momentum couplings of two-particles or two-holes are indicated by a horizontal bracket. ϵ_F represents the Fermi energy. The unperturbed energies $\mathcal{E}_{j_p j_n}$ are given in MeV, being the PBCS results given in brackets.

corresponds to a 1p1h state in ^{12}N , $|1p_{3/2}1p_{3/2}\rangle$ and $|1p_{1/2}1p_{1/2}\rangle$ correspond to 2p2h states, and $|1p_{3/2}1p_{1/2}\rangle$ to a 3p3h state in the same nucleus. Therefore one can expect that the energy ordering of these states were given by (4.3), with $\Delta = \Delta_{\text{ls}} - \Delta_{\text{pair}}$ being the energy difference between the spin-orbit splitting, Δ_{ls} , and the pairing energy, Δ_{pair} . A similar discussion is pertinent to the remaining three nuclei ^{10}B , ^{14}N , and ^{12}B . That is, one expects that their lowest states would be, respectively, $|1p_{3/2}1p_{3/2}\rangle$, $|1p_{1/2}1p_{1/2}\rangle$ and $|1p_{3/2}1p_{1/2}\rangle$, as it happens in the PBCS case but not within the BCS. Finally, it could be worthwhile to indicate that the same pn quasiparticle excitation has quite different ph compositions in different nuclei. This can be observed by scrutinizing the four columns in Fig. 3.

The improvement introduced by the PBCS can also be visualized by making a direct calculation of the unperturbed GT strength in ^{12}N , given by

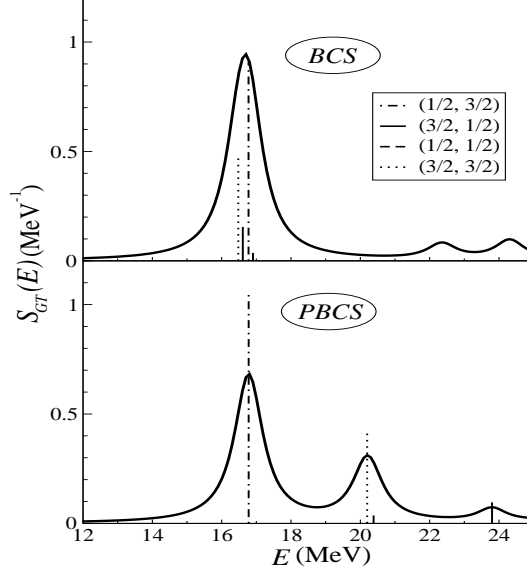


FIG. 4: The BCS (upper panel) and the PBCS (lower panel) Gamow-Teller strength function in ^{12}N .

$$S_{GT}(E) \equiv \frac{1}{\pi} \sum_{pn} |g_A \langle p || \sigma || n \rangle|^2 \frac{\eta}{\eta^2 + (E - \mathcal{E}_{j_p j_n})^2}. \quad (4.4)$$

The BCS and PBCS results for ^{12}N , when folded with a with $\eta = 1$ MeV, are compared in Fig. 4. The PBCS energy ordering, given by (4.3), is accompanied by the partial shifting of the GT strength to higher energies. Therefore it can be said that within the PBCS the GT resonance is quenched even at the level of the mean field.

In view of the above mentioned disadvantages of the standard BCS approach, the number projection results will be discussed mainly from now on. In our previous work [14] we have also pointed out that the values of the coupling strengths v_s and v_t within the particle-particle (pp) and particle-hole (ph) channels which are used in $N > Z$ nuclei ($v_s^{pp} \equiv v_s^{pair}$, and $v_t^{pp} \gtrsim v_s^{pp}$), might not be suitable for $N = Z$ nuclei. In fact, the best agreement with data in ^{12}C was obtained when the pp channel is totally switched off, *i.e.*, $v_s^{pp} \equiv v_t^{pp} = 0$, and three different set of values for the ph coupling strengths have been suggested in Ref. [14], namely:

Parametrization I: $v_s^{ph} = v_s^{pair} = 24$ MeV-fm³, and $v_t^{ph} = v_s^{ph}/0.6 = 40$ MeV-fm³,

Parametrization II: $v_s^{ph} = 27$ MeV-fm³, and $v_t^{ph} = 64$ MeV-fm³, and

Parametrization III: $v_s^{ph} = v_t^{ph} = 45$ MeV-fm³.

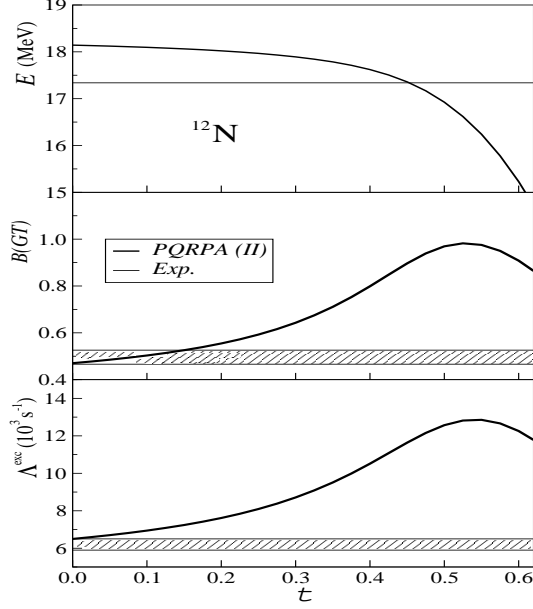


FIG. 5: The PQRPA calculations, as function of the pp parameter t , are confronted with the experimental data taken from Refs. [24, 25, 26] for: 1) the energy difference ω_{1+} between the 1^+ ground state in ^{12}N and the 0^+ ground state in ^{12}C (upper panel), 2) the B -value for the GT beta transition between these two states (middle panel), and 3) the corresponding muon capture rate $\Lambda(1_1^+)$ (lower panel). The values of v_s^{ph} and v_t^{ph} correspond to *Parametrization II*.

The results displayed in Fig. 5 suggest that the choice $v_t^{pp} = 0$ for the pp parameter in the $S = 0, T = 1$ channel could be appropriate for the description of the $N = Z$ nuclei. The calculations are shown as functions of the parameter

$$t = \frac{2v_t^{pp}}{v_s^{pair}(p) + v_s^{pair}(n)},$$

together with the experimental data for: 1) the energy difference ω_{1+} between the 1^+ ground state in ^{12}N and the 0^+ ground state in ^{12}C , 2) the B -value for the GT beta transition between these two states, and 3) the corresponding exclusive muon capture rate $\Lambda(1_1^+) \equiv \Lambda^{\text{exc}}$. The values of v_s^{ph} and v_t^{ph} are that from the *Parametrization II*, but quite similar results are obtained with other two sets of parameters. Note that the ph interaction first shifts the energy ω_{1+} upwards by ~ 1.5 MeV, from its unperturbed value $\mathcal{E}_{1p_{3/2}1p_{3/2}} = 16.8$ MeV. Then, when t is increased, we have an opposite attractive effect. That is, the pp interaction diminishes ω_{1+} all up to $t \gtrsim 0.6$, where the well known collapse of the QRPA approximation occurs. At variance with what happens in the case of heavy nuclei, here

the values of $B(GT)$ and $\Lambda(1_1^+)$ basically rise with t , and the agreement with the data is achieved only when the pp interaction is totally switched off. Quite generally the nuclear moments (2.34) also depend weakly on the $S = 1, T = 0$ channel parameter v_s^{pp} , for which we adopt as well the null value, just to be consistent with our election of v_t^{pp} .

TABLE V: Experimental and calculated muon capture rate in units of 10^3 s^{-1} . The full PQRPA calculations, which include the relativistic corrections are listed for all three parametrizations I, II, and III. Theoretical results that involve only the velocity-independent matrix elements are displayed in parentheses in the third column just for the case II. The rates are grouped by their degrees of forbiddenness. There are exhibited: i) the exclusive rates $\Lambda(J_f^\pi)$, for $J_f^\pi = 1_1^+, 1_1^-, 2_1^-, 2_1^+$, ii) the multipole decomposition of the rates $\sum_f \Lambda(J_f^\pi)$ for each final state with spin and parity J_f^π , and iii) the inclusive decay rate $\Lambda^{\text{inc}} \equiv \sum_{J_f^\pi} \Lambda(J_f^\pi)$. In column four are listed the results of recent shell-model calculations, which are explained in the text. The measured capture rates are given in the last column.

μ capture rate	PQRPA			Shell Model			Experiment
	(I)	(II)	(III)	SM1[16]	SM2[16]	SM3[17]	
<u>allowed</u>	49.3 %			39.3 %			
$\Lambda(1_1^+)$	7.52	6.27(6.50)	6.27	11.56	6.3	6.0	6.2 ± 0.3 [26]
$\sum_f \Lambda(0_f^+)$	3.68	2.86 (3.15)	3.77	0.21			
$\sum_f \Lambda(1_f^+)$	20.28	18.14 (18.63)	18.22	15.43			
<u>1st forbidden</u>	46.6 %			55.7 %			
$\Lambda(1_1^-)$	1.06	0.49 (0.51)	0.98			1.86	0.62 ± 0.20 [27, 28]
$\Lambda(2_1^-)$	0.31	0.18 (0.18)	0.16			0.22	0.18 ± 0.10 [27, 28]
$\sum_f \Lambda(0_f^-)$	2.62	2.35 (0.72)	2.35	2.12			
$\sum_f \Lambda(1_f^-)$	11.84	10.37 (9.51)	11.37	12.25			
$\sum_f \Lambda(2_f^-)$	7.78	7.12 (6.90)	7.15	7.79			
<u>2nd forbidden</u>	3.9 %			4.6 %			
$\Lambda(2_1^+)$	0.19	0.14 (0.16)	0.15			0.25	0.21 ± 0.10 [27, 28]
$\sum_f \Lambda(2_f^+)$	1.26	1.09 (0.89)	1.17	1.36			
$\sum_f \Lambda(3_f^+)$	0.63	0.57 (0.57)	0.58	0.46			
Λ^{inc}	48.16	42.56 (40.7)	44.67	39.82	42.2	33.5	38 ± 1 [29]

TABLE VI: Experimental and calculated flux-averaged cross section for the $^{12}\text{C}(\nu_e, e^-)^{12}\text{N}$ DAR reaction in units of 10^{-42} cm². The full PQRPA calculations, which include the relativistic corrections are listed for all three parametrizations I, II, and III. Theoretical results that involve only the velocity-independent matrix elements are displayed in parentheses just for the case II in the third column. The multipole decomposition $\sum_f \bar{\sigma}_e(J_f^\pi)$ for each final state with spin and parity J_f^π , as well as the exclusive, $\bar{\sigma}_e^{\text{exc}} \equiv \sigma_e(J_f^\pi = 1_1^+)$, and inclusive $\bar{\sigma}_e^{\text{inc}} = \sum_{J_f^\pi} \bar{\sigma}_e(J_f^\pi)$ cross sections, are shown. In column four are listed the results of a recent shell-model calculations, which are explained in the text. The measured cross section are given in the last column.

(ν_e, e^-) cross section	PQRPA			Shell Model			Experiment	
	(I)	(II)	(III)	SM1[16]	SM2[16]	SM3[17]		
<u>allowed</u>	83.0 %			83.6 %			$8.9 \pm 0.3 \pm 0.9$ [4]	
$\bar{\sigma}_e(1_1^+)$	9.94	8.07 (8.00)	8.17	20.86	7.9	9.3		
$\sum_f \bar{\sigma}_e(0_f^+)$	1.92	1.35 (1.31)	2.01	0.00				
$\sum_f \bar{\sigma}_e(1_f^+)$	15.98	14.08 (14.22)	12.14	22.52				
<u>1st forbidden</u>	16.6 %			16.0 %				
$\sum_f \bar{\sigma}_e(0_f^-)$	0.07	0.07 (0.05)	0.07	0.04				
$\sum_f \bar{\sigma}_e(1_f^-)$	1.94	1.59 (1.43)	1.80	1.90				
$\sum_f \bar{\sigma}_e(2_f^-)$	1.66	1.43 (1.41)	1.44	2.36				
<u>2nd forbidden</u>	0.4 %			0.4 %				
$\sum_f \bar{\sigma}_e(2_f^+)$	0.07	0.05 (0.04)	0.05	0.08				
$\sum_f \bar{\sigma}_e(3_f^+)$	0.03	0.03 (0.03)	0.03	0.03				
$\bar{\sigma}_e^{\text{inc}}$	21.67	18.60 (18.49)	17.54	26.93	12.5	15.1		$13.2 \pm 0.4 \pm 0.6$ [4]

Results for the muon capture rates, and the neutrino (ν_e, e^-) DAR, and (ν_μ, μ^-) DIF reaction flux-averaged cross sections are shown, respectively, in Tables V, Tables VI and Tables VII.

The flux-averaged cross section is defined as

$$\bar{\sigma}_\ell(J_f) = \int_{\Delta_{J_f}} dE_\nu \sigma_\ell(E_\nu, J_f) \Phi_\ell(E_\nu); \quad \ell = e, \mu, \quad (4.5)$$

where $\Phi_\ell(E_\nu)$ is the normalized neutrino flux. For electron neutrinos this flux was approximated by the Michel spectrum, and for the muon neutrinos we used that from Ref. [30].

TABLE VII: Idem Table VI but for the averaged cross section $^{12}C(\nu_\mu, \mu^-)^{12}N$ DIF reaction in units of 10^{-40} cm^2 .

(ν_μ, μ^-) cross section	PQRPA			Shell Model			Experiment
	(I)	(II)	(III)	SM1[16]	SM2[16]	SM3[17]	
<u>allowed</u>	20.0 %			17.1 %			$0.56 \pm 0.08 \pm 0.10$ [5]
$\bar{\sigma}_\mu(1_1^+)$	0.74	0.59 (0.56)	0.59	1.16	0.56	0.9	
$\sum_f \bar{\sigma}_\mu(0_f^+)$	0.37	0.26 (0.26)	0.39	0.11			
$\sum_f \bar{\sigma}_\mu(1_f^+)$	2.68	2.33 (2.40)	2.34	2.95			
<u>1st forbidden</u>	39.5 %			36.4 %			
$\sum_f \bar{\sigma}_\mu(0_f^-)$	0.03	0.04 (0.07)	0.04	0.07			
$\sum_f \bar{\sigma}_\mu(1_f^-)$	3.34	2.79 (2.84)	3.10	3.55			
$\sum_f \bar{\sigma}_\mu(2_f^-)$	2.53	2.28 (2.13)	2.29	2.91			
<u>2nd forbidden</u>	27.1 %			22.2 %			
$\sum_f \bar{\sigma}_\mu(2_f^+)$	2.55	2.28 (2.11)	2.37	2.59			
$\sum_f \bar{\sigma}_\mu(3_f^+)$	1.34	1.23 (1.29)	1.23	1.39			
<u>3th forbidden</u>	10.2 %			17.7 %			
$\sum_f \bar{\sigma}_\mu(3_f^-)$	0.74	0.69 (0.73)	0.71	1.77			
$\sum_f \bar{\sigma}_\mu(4_f^-)$	0.68	0.63 (0.63)	0.63	1.41			
<u>4th forbidden</u>	3.1 %			6.5 %			
$\sum_f \bar{\sigma}_\mu(4_f^+)$	0.22	0.21 (0.20)	0.21	0.66			
$\sum_f \bar{\sigma}_\mu(5_f^+)$	0.20	0.19 (0.19)	0.19	0.51			
$\bar{\sigma}_\mu^{\text{inc}}$	14.69	12.94 (12.86)	13.51	17.92	13.8	19.2	$10.6 \pm 0.30 \pm 1.80$ [5]

The energy integration is carried out in the DAR interval $m_e + \omega_{J_f} \leq \Delta_{J_f}^{\text{DAR}} \leq 52.8$ MeV for electrons and in the DIF interval $m_\mu + \omega_{J_f} \leq \Delta_{J_f}^{\text{DIF}} \leq 300$ MeV for muons.

The full PQRPA calculations, which include the relativistic corrections are listed for all three parametrizations I, II, and III. On the contrary, the theoretical results involving just the velocity-independent operators $Y_J(\kappa\mathbf{r})$ and $S_{JL}(\kappa\mathbf{r})$ are displayed only for the case II. Contributions of the other two operators, $P_{JL}(\kappa\mathbf{r})$ and $Y_J(\kappa\mathbf{r}, \boldsymbol{\sigma} \cdot \mathbf{v})$, to the muon capture rates are small (of the order of 5%) as displayed in Table V. The only exception are the 0^-

states where the relativistic operator $Y_0(\kappa\mathbf{r}, \boldsymbol{\sigma} \cdot \mathbf{v})$ dominates over the non-relativistic one $S_{01}(\kappa\mathbf{r})$. We also see from Tables VI and VII that the nonlocality effects on the neutrino-nucleus reactions are of the order of 1% and therefore they can be neglected.

The numerical results are ordered by following the forbiddenness of the corresponding transition moments, which can be: *allowed* (A): $J^\pi = 0^+, 1^+$, *first forbidden* (F1): $J^\pi = 0^-, 1^-, 2^-$, *second forbidden* (F2): $J^\pi = 2^+, 3^+$, *third forbidden* (F3): $J^\pi = 3^-, 4^-$, and so on. The response of the three weak processes to successive multipoles is strongly correlated with the average momentum transfer, $\bar{\kappa}$, involved in each: (ν_e, e^-) -reaction, $\bar{\kappa} \sim 0.2 \text{ fm}^{-1}$; μ -capture, $\bar{\kappa} \sim 0.5 \text{ fm}^{-1}$; and (ν_μ, μ^-) -reaction, $\bar{\kappa} \sim 1 \text{ fm}^{-1}$. As a consequence, in the first case the A-moments are by far the dominant ones, contributing with $\sim 83.0\%$, with the remaining part of the reaction strength carried almost entirely ($\sim 16.6\%$) by the F1-moments. For μ -capture, the A- and F1-matrix elements contribute, respectively, with 49.3% and 46.6%, while the F2-moments carry only 3.9% of the total transition rate, and the contribution of the F3-ones are negligible small. Finally, the inclusive cross section in the (ν_μ, μ^-) -reaction is spread out rather uniformly over several multipoles and it is necessary to include up to fourth forbidden moments, being their intensities distributed as: 20.0% (A), 39.5% (F1), 27.1% (F2), 10.2% (F3), and 3.1% (F4). The exclusive contributions, coming from the ground state 1_1^+ , are quite different in the three cases due to the just mentioned implication of the momentum transfer. They are 43%, 15%, and 5%, respectively, of the total transition rates for the (ν_e, e^-) -reaction, μ -capture, and (ν_μ, μ^-) -reaction.

Let us say a few words on the comparison of our results with the experimental data:

- μ capture (Table V): All exclusive rates $\Lambda(J^\pi)$ with $J_f^\pi = 1_1^+, 1_1^-, 2_1^-, 2_1^+$, are fairly well accounted for by the theory, while the inclusive rate, Λ^{inc} , is overpredicted by $\sim 10\%$.
- (ν_e, e^-) -reaction (Table VI): Even though the exclusive cross section, $\bar{\sigma}_e^{\text{exc}}$, is well reproduced within the PQRPA, the inclusive one, $\bar{\sigma}_e^{\text{inc}}$, is $\sim 40\%$ above the data. It is important to mention that the value of $\bar{\sigma}_e^{\text{inc}}$ is very sensitive to the strength distribution of low-lying excited states within the DAR energy interval, $18 \text{ MeV} \lesssim E_\nu \lesssim 50 \text{ MeV}$, because the electron-neutrino flux, $\Phi_e(E_{\nu_e})$, changes there very abruptly.
- (ν_μ, μ^-) -reaction (Table VII): Here the inclusive cross section is in full agreement with the data, whereas the exclusive one is overpredicted by a $\sim 20\%$.

In the last three tables we also confront our PQRPA results with the shell model calculations performed by: a) Hayes and Towner [16], within the model spaces called by them as (iii) and (iv), and which are labeled here, respectively, as SM1 and SM2, and b) Auerbach and Brown [17] which we label as SM3. The multipole breakdown in the contributions to the cross sections from each multipole is only given for the SM1 scheme [16], which is in fairly good agreement with our results, as can be inferred from the comparison of the percentages displayed in Tables V, VI, and VII. The concordance is particularly significant for the μ -capture rates, where, as seen from Table V, the major discrepancy is in the Fermi transitions, for which we get $\sum_f \Lambda(0_f^+) = 2.86$ while they only get 0.21 (in units of 10^3 s^{-1}). We don't find any explanation for this fact. Other important difference appears in the values of the exclusive 1_1^+ -transition rates for all three observables, as well as the inclusive cross sections, for both electron and muon-neutrinos, which are overestimated within the SM1 by a factor of ~ 2 in comparison with data. In the SM2 the agreement with the measurements is quite reasonable and the concordance with the present calculations is significantly better. Regarding the comparison with the calculations SM3, done by Auerbach and Brown [17], it can be said that their exclusive μ -capture rates agree fairly well with ours, as well as their inclusive cross section $\bar{\sigma}_e^{\text{inc}}$, but that they underestimate Λ^{inc} and overestimate $\bar{\sigma}_\mu^{\text{inc}}$.

In the DIF neutrino oscillation search [1] an excess signal of

$$N_{\nu_\mu \rightarrow \nu_e}^{\text{exp}} = 18.1 \pm 6.6 \pm 4.0,$$

events has been observed in the $^{12}\text{C}(\nu_e, e^-)^{12}\text{N}$ reaction, which are evaluated theoretically by the expression

$$N_{\nu_\mu \rightarrow \nu_e}^{\text{th}} = \int_{\Delta^{\text{osc}}} dE_\nu \sigma_e(E_\nu) P_{\nu_\mu \rightarrow \nu_e}(E_\nu) \Phi_\mu(E_\nu); \quad \sigma_e(E_\nu) \equiv \sum_{J_f} \sigma_e(E_\nu, J_f),$$

where $77.3 \text{ MeV} \leq \Delta^{\text{osc}} \leq 217.3 \text{ MeV}$ stands for the experimental energy window. The oscillation probability reads

$$P_{\nu_\mu \rightarrow \nu_e}(E_\nu) = \sin^2(2\theta) \sin^2\left(\frac{1.27\Delta m^2 L}{E_\nu}\right),$$

where θ is the mixing angle between the neutrino mass eigenstates, Δm^2 is the difference in neutrino eigenstate masses squared, in eV^2 , and L is the distance in meters traveled by the neutrino from the source. One sees therefore that the extraction of the permitted values of θ and Δm^2 from experimental data might depend critically on the theoretical estimate of

$\sigma_e(E_\nu)$. In the analysis performed so far [1] has been used the electron cross section from the calculation done within the continuum random phase approximation (CRPA) [31], which is compared with the present results in Figure 6. As can be noticed the PQRPA yields a substantially different $\sigma_e(E_\nu)$, inside the experimental energy window for the neutrino energy. The consequences of this difference on the confidence regions for $\sin^2(2\theta)$ and Δm^2 will be discussed in a future paper.

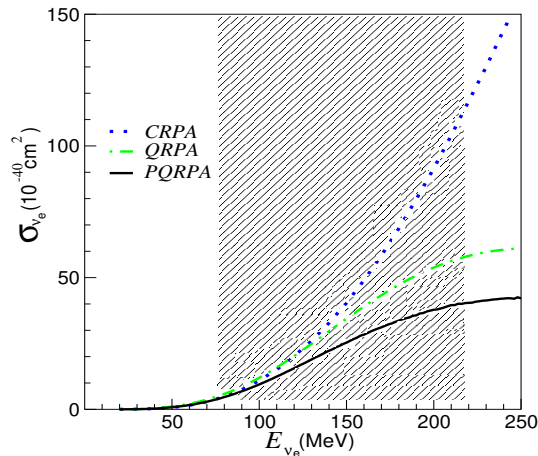


FIG. 6: Calculated cross section σ_{ν_e} as function of the neutrino energy. The dashed region indicates the experimental energy window.

-
- [1] LSND Collaboration, C. Athanassopoulus *et al.*, Phys. Lett. **81**, 1774 (1998); Phys. Rev. C **58**, 2489 (1998).
 - [2] LSND Collaboration, A. Aguilar *et al.*, Phys. Rev. D **64**, 112007 (2001).
 - [3] KARMEN Collaboration, K. Eitel *et al.*, Nucl. Phys. B, Proc.Suppl. **77**, 212 (1999).
 - [4] LSND Collaboration, L-B. Auerbach *et al.*, Phys. Rev. C **64**, 065501 (2001).
 - [5] LSND Collaboration, L-B. Auerbach *et al.*, Phys. Rev. C **66**, 015501 (2002).

- [6] T.W. Donnelly and W.C. Haxton, *Atomic Data and Nuclear Data Tables* **23**, 103 (1979);
T.W. Donnelly and R. D. Peccei, *Phys. Rep.* **50**, 1 (1979).
- [7] J.D. Walecka, *Theoretical Nuclear and Subnuclear Physics, Oxford University Press, New York*, 531 (1995).
- [8] N. Auerbach, N. Van Giai, and O.K. Vorov, *Phys. Rev. C* **56**, 2368 (1997).
- [9] C. Volpe, N. Auerbach, G. Colò, T. Suzuki, and N. Van Giai, *Phys. Rev. C* **62**, 015501 (2000).
- [10] T. Kuramoto, M. Fukigita, Y. Kohyama and K. Kubodera, *Nucl. Phys. A* **512**, 711 (1990).
- [11] J.R.Luyten, H.P.C. Rood and H.A. Tolhoek, *Nucl.Phys.* **41**, 236 (1963).
- [12] N. Auerbach and A. Klein, *Nucl. Phys. A* **395**, 77 (1983).
- [13] C. Barbero, F. Krmpotić, and D. Tadić, *Nucl. Phys. A* **628**, 170 (1998); C. Barbero, F. Krmpotić, A. Mariano and D. Tadić, *Nucl. Phys. A* **650**, 485 (1999).
- [14] F. Krmpotić, A. Mariano, and A. Samana, *Phys. Lett. B* **541**, 298 (2002).
- [15] I. Supek, *Teorijska Fizika i Struktura Materije*, (Zagreb), Vol. II (1964).
- [16] A.C. Hayes and I.S. Towner, *Phys. Rev. C* **61**, 044603 (2000).
- [17] N. Auerbach and B.A. Brown, *Phys. Rev. C* **65**, 024322 (2002).
- [18] R.J. Blin-Stoyle and S.C.K. Nair, *Adv. Phys.* **15**, 493 (1966).
- [19] I.S. Towner and J.C. Hardy, *The Nucleus as a Laboratory for Studying Symmetries and Fundamental Interactions*, eds. E.M. Henley and W.C. Haxton, nucl-th/9504015.
- [20] F. Krmpotić, A. Mariano, T.T.S. Kuo, and K. Nakayama, *Phys. Lett. B* **319**, 393 (1993).
- [21] J. Hirsch and F. Krmpotić, *Phys. Rev. C* **41**, 792 (1990).
- [22] J. Hirsch and F. Krmpotić, *Phys. Lett. B* **246**, 5 (1990).
- [23] F. Krmpotić, J. Hirsch and H. Dias, *Nucl. Phys. A* **542**, 85 (1992).
- [24] F. Ajzenberg-Selove, *Nucl. Phys. A* **433**, 1 (1985).
- [25] D. E. Alburger and A.M. Nathan, *Phys. Rev. C* **17**, (1978) 280.
- [26] G. H. Miller *et al.*, *Phys. Lett. B* **41**, 50 (1972).
- [27] D.F. Measday, *Phys. Rep.* **354**, 243 (2001).
- [28] T.J. Stocki, D.F. Maesday, E. Gete, M.A. Saliba, and T.P. Gorrinde, *Nucl. Phys. A* **697**, 55 (2002).
- [29] T Suzuki *et al.*, *Phys. Rev. C* **35**, 2212 (1987).
- [30] LSND home page, <http://www.nu.to.infn.it/exp/all/lsnd/>
- [31] E. Kolbe, K. Langanke, and P. Vogel, *Nuc. Phys. A* **652**, 91 (1999).

[32] To avoid confusion, we will be using roman fonts (M,m) for masses and math italic fonts (M,m) for azimuthal quantum numbers.

[33] We note that there are misprints in [14, (23)].